Pervasive aerobic nitrogen cycling in the surface ocean across the Paleoproterozoic Era

Michael A. Kipp[a,b,*], Eva E. Stüeken[b,c], Misuk Yun[d], Andrey Bekker[e,f], and Roger Buick[a,b]

[a]*Department of Earth & Space Sciences and Astrobiology Program, University of Washington, Seattle, WA 98195, USA*

[b]*Virtual Planetary Laboratory, NASA Astrobiology Institute, Seattle, WA 98195, USA*

[c]*School of Earth & Environmental Sciences, University of St. Andrews, KY16 9AL, Scotland, United Kingdom*

[d]*Department of Geological Sciences, University of Manitoba, Winnipeg, Manitoba, R3G 2K4 Canada*

[e]*Department of Earth Sciences, University of California, Riverside, CA 92521, USA*

[f]*Department of Geology, University of Johannesburg, P.O. Box 524, Auckland Park, 2006, Republic of South Africa*

*correspondence: kipp@uw.edu, Johnson Hall Room 070, Dept. of Earth & Space Sciences, University of Washington, 4000 NE 15th Ave, Seattle, WA, USA, 91895-1310

Keywords: Paleoproterozoic, nitrogen isotopes, paleoredox, eukaryote evolution, Great Oxidation Event, Lomagundi Event

Abstract

Nitrogen isotope ratios in marine sedimentary rocks have become a widely used biogeochemical proxy that records information about nutrient cycling and redox conditions in Earth's distant past. While the past two decades have seen considerable progress in our understanding of the Precambrian sedimentary nitrogen isotope record, it is still compromised by substantial temporal gaps. Furthermore, quantitative links between nitrogen isotope data, marine redox conditions, and nutrient availability are largely lacking in a Precambrian context. Here we present new nitrogen isotope data from a suite of marine sedimentary rocks with ca. 2.4 to 1.8 Ga ages, spanning the Great Oxidation Event in the Paleoproterozoic, to better constrain the response of the nitrogen cycle to the first major redox transition in Earth's history. We further construct a simple box model to describe the major pathways that influenced the nitrogen isotope mass balance of the Precambrian ocean and use this as a platform to evaluate the Precambrian nitrogen isotope record. Within this framework, we find that consistently positive nitrogen isotope values, ranging from +1.1 to +7.7‰, across the early Paleoproterozoic are strong evidence for an expansion of oxygenated surface waters. Since the isotopic signature of aerobic nitrogen cycling is recorded in the biomass of nitrate-assimilating organisms, this implicates widespread nitrate bioavailability in this time interval. The decline in offshore nitrogen isotope ratios in the Mesoproterozoic is consistent with the contraction of oxic waters, which could have inhibited the expansion of nitrate-fueled ecosystems to pelagic waters until the widespread oxygenation of the ocean in the latest Neoproterozoic to early Phanerozoic.

1. Introduction

At the beginning of the Paleoproterozoic Era, Earth's atmosphere underwent a permanent shift from a reducing to an oxidizing state. This transition – termed the "Great Oxidation Event" (GOE) – began by ca. 2.43 Ga (Gumsley et al., 2017) and was characterized by oxygen-rich marine and terrestrial settings lasting until ca. 2.06 Ga (Bekker and Holland, 2012). In the aftermath of the GOE, atmospheric oxygen fell to an intermediate level that was substantially higher than in the Archean, but lower than Phanerozoic concentrations (Lyons et al., 2014). While the exact timing and mechanism of the GOE remain debated, the magnitude of its implications is clear: the biogeochemical pathways operating at Earth's surface were dramatically and permanently altered (Lyons et al., 2014), and the stage was set for the emergence of aerobically-respiring organisms, including the first eukaryotes (Javaux and Lepot, 2018).

Several paleo-redox proxies have been used to characterize the transition toward oxygenated surface environments in the Paleoproterozoic. Early evidence from oxidized paleosols documented the influence of atmospheric oxygen in weathering environments by ca. 2.2 Ga (e.g. Beukes et al., 2002), and the recognition of a large perturbation in the global carbon cycle through carbon isotope systematics of carbonates has long been used to support a notion of extreme oxygen production during the GOE (e.g. Karhu and Holland, 1996). More recently, the disappearance of mass-independent fractionation of sulfur isotopes (MIF-S) has been used to pinpoint the crossing of a threshold of 10^{-5} times the present atmospheric level of oxygen (PAL) between 2.46 and 2.32 Ga (Farquhar et al., 2000; Gumsley et al., 2017; Luo et al., 2016; Bekker et al., 2004), which has come to define the onset of the GOE proper.

63 The redox states of the atmosphere and ocean are coupled on geologic timescales, and
64 so the rise of atmospheric oxygen, the "oxygen overshoot," and the subsequent deoxygenation
65 should have considerably affected marine redox chemistry. Indeed, enrichments of redox-
66 sensitive trace elements in organic-rich shales implicate an expansion of oxygenated seawater
67 during the GOE (Scott et al., 2008; Partin et al., 2013; Kipp et al., 2017), as do sulfur isotope ratios
68 in marine sedimentary rocks, which suggest a waxing and waning seawater sulfate reservoir
69 (Planavsky et al., 2012; Scott et al., 2014). Beyond these converging lines of evidence for
70 widespread ocean oxygenation during the GOE, recent work has begun to decipher even regional
71 redox gradients. Highly positive selenium isotope ratios in offshore marine sediments during the
72 GOE imply oxygenated surface oceans, with anoxia prevailing at depth (Kipp et al., 2017). This
73 finding is corroborated by the record of iodine enrichment in shallow-marine carbonates
74 deposited at the same time, which requires at least mildly oxygenated surface waters (Hardisty
75 et al., 2017).
76 Nitrogen isotope geochemistry can bring additional perspective to bear on the question
77 of basinal redox structure, as nitrogen has a high redox potential – similar to that of selenium
78 and iodine – and is sensitive to redox conditions in the photic zone, where primary productivity
79 is highest. The nitrogen isotope composition of organic matter in offshore marine sediments can
80 thus speak to redox chemistry in the photic zone overlying the outer shelf and open ocean.
81 Furthermore, as nitrogen is an essential macronutrient, nitrogen isotopes in marine sediments
82 also record the balance between nitrogen-fixing organisms (strictly prokaryotic) and nitrogen-
83 assimilating organisms (which can be either prokaryotic or eukaryotic). Since nitrate (NO_3^-) is the
84 preferred nitrogenous substrate for eukaryotes in the modern ocean (e.g. Karl et al., 2001),

tracing the prevalence of aerobic nitrogen cycling during the Paleoproterozoic can both constrain redox conditions and speak directly to the bioavailability of NO_3^- for eukaryotic organisms.

Notably, despite the wealth of evidence from a variety of well-established paleo-redox proxies, the immediate response of the nitrogen cycle to the GOE has only been investigated in a few studies that focused specifically on the onset, culmination, or aftermath of the GOE (Kump et al., 2011; Luo et al., 2018; Papineau et al., 2009; Zerkle et al., 2017). While those studies have provided important evidence for the presence of aerobic nitrogen cycling during the GOE, the sparse record through the Paleoproterozoic hinders reconstructions of global temporal and spatial patterns across the proposed "oxygen overshoot."

Here we present nitrogen isotope data from a suite of Paleoproterozoic marine sedimentary rocks that span the GOE in order to better characterize the response of the biogeochemical nitrogen cycle to the first permanent increase in atmospheric and marine oxygen levels. Taking this a step further, we then construct a simple steady-state isotope box model and use it as a platform for evaluating secular trends in the Precambrian nitrogen isotope record. To date, nitrogen isotopes in ancient marine sediments have been used at best as a semi-quantitative redox proxy. We find that even with this simple view of the nitrogen cycle, a robust correlation can be drawn between nitrogen isotope ratios in marine sediments and the extent of oxic surface waters. This new, quantitative framework for interpreting the nitrogen isotope record enables a direct comparison with results from other proxies, thereby refining our view of ocean oxygenation during and after the GOE.

2. Materials

We collected nitrogen and organic carbon isotopic data from a large sample set (n=144) of marine, siliciclastic sedimentary rocks with ages spanning ca. 2.4 to 1.8 Ga. We targeted shales deposited in offshore depositional environments (below wave base) in basins that were open with respect to exchange with the global ocean. When viewed together, these lithologies capture a representative view of secular trends in global nitrogen cycling. None of the units studied here have experienced metamorphism beyond lower greenschist facies. Detailed descriptions of individual units can be found in the Supplementary Materials.

3. Methods

3.1 Sample preparation for bulk rock analyses

Sample preparation followed published methods (Stüeken, 2013; Koehler et al., 2017). Samples were crushed into centimeter-sized chips, and equipment was cleaned between samples with methanol and 18 MΩ DI-H_2O. Rock chips were sequentially cleaned with ethanol, 2N HCl, and DI-H_2O to remove modern contaminants, then dried in an oven at 60°C. Clean chips were pulverized using an aluminum oxide puck mill that was cleaned between samples using methanol, DI-H_2O, and pre-combusted (500°C) silica sand. Prior to analysis, powders were decarbonated using 6N HCl, then rinsed with DI-H_2O and dried in an oven at 60°C.

3.2 Kerogen extraction

Kerogen was extracted from bulk rock powders following published protocols (Stüeken et al., 2015). Rock powders were weighed out into teflon bottles and treated with a 50:50 mixture of DI-H_2O and concentrated (29N) hydrofluoric acid (HF) in a shaking water bath at 55°C.

Digests were then centrifuged and the supernatant was decanted. A BF_3 solution (62.5g H_3BO_3, 100 mL DI-H_2O, 100 mL 29N HF) was then added, and the samples were placed in a shaking water bath at 55°C to dissolve remaining fluoride minerals. Samples were then centrifuged, the supernatant was decanted, and the samples were washed with three iterations of DI-H_2O. The isolated kerogen was transferred to a combusted pyrex vial in DI-H_2O and freeze-dried to remove all moisture prior to analysis.

3.3 Isotopic analyses

The isotopic composition ($\delta^{15}N$ and $\delta^{13}C_{org}$) of decarbonated powders and kerogen isolates was measured on a Costech™ ECS 4010 Elemental Analyzer coupled to a Thermo Finnigan™ MAT253 continuous flow isotope-ratio mass spectrometer housed in IsoLab at the Department of Earth & Space Sciences, University of Washington. Combustion was carried out with 20ml O_2 at 1000°C. A magnesium perchlorate trap was used to remove water from the gas stream. Isotopic measurements were standardized against three in-house standards (two glutamic acids "GA1" and "GA2", and dried salmon "SA"), which are calibrated to international reference materials USGS40 and USGS41. An aliquot of the Neoarchean Mt. McRae Shale was analyzed as an in-house standard to test long-term precision. Isotopic data are reported in delta notation relative to air for nitrogen and Vienna PeeDee Belemnite (V-PDB) for carbon.

Analytical blanks resulting from combustion were monitored and subtracted from nitrogen data; blanks were negligible for carbon measurements. Average analytical accuracy of $\delta^{15}N$ among individual runs, based on in-house standard "GA1" was -0.03 ± 0.19‰ (1σ). Accuracy of $\delta^{13}C_{org}$ measurements based on in-house standard "SA" was -0.05 ± 0.07‰ (1σ). The average

analytical precision among all runs based on in-house standard "UW-McRae" was 0.12‰ (1σ) for $\delta^{15}N$ and 0.04‰ (1σ) for $\delta^{13}C_{org}$. All samples were analyzed at least twice, with an average standard deviation between sample replicates of 0.25‰ for $\delta^{15}N$ and 0.17‰ for $\delta^{13}C_{org}$.

Samples from the Sengoma Argillite Formation were analyzed for bulk nitrogen content and $\delta^{15}N_{bulk}$ values (without decarbonation) following standard procedures in the Stable Isotopes for Innovative Research Laboratory at the Department of Geological Sciences, University of Manitoba (cf. Zerkle et al., 2017). Analyses were performed using a Costech™ 4010 Elemental Analyzer coupled to a Thermo Finnigan™ Delta V Plus isotope-ratio mass spectrometer. A magnesium perchlorate-carbosorb trap was placed before ConFlo III to remove water and CO_2. Temperature in the oxidation column was raised to 1050°C for efficient sample combustion, and a 'macro' O_2 injection loop was utilized. CO_2 levels were monitored during analytical sessions. Sample normalization was performed using two-point calibration with two international standards (USGS40 and USGS41) at the beginning, middle, and end of each run. To monitor the quality of analytical performance, two certified standards were analyzed alongside with samples: B2153, soil, % TN = 0.13 ± 0.02%, $\delta^{15}N$ = +6.70 ± 0.15‰ (Elemental Microanalysis); and SDO-1, Devonian Ohio Shale, % TN = 0.36 ± 0.01%, $\delta^{15}N$ = -0.8 ± 0.3‰ (USGS). The data obtained were TN (wt. %) = 0.14 ± 0.00% and $\delta^{15}N$ values of +6.76 ± 0.02‰ (n=3) for B2153, and TN (wt. %) = 0.37 ± 0.00% and $\delta^{15}N$ values of -0.32 ± 0.02‰ (n=3) for SDO-1.

3.4 Isotope box model

We constructed a steady-state box model of the nitrogen cycle to track the salient processes affecting nitrogen isotope mass balance in the ocean system (Fig. 1). The major input of nitrogen

173 to the ocean is biological N_2 fixation to NH_4^+, which is released during biomass degradation and
174 oxidized rapidly to NO_3^- (nitrification). We assumed that nitrification occurs instantaneously as
175 soon as NH_4^+ upwells to the surface ocean, because previous studies have shown that nitrification
176 proceeds even at nanomolar levels of dissolved O_2 (e.g. Kalvelage et al., 2011). The major output
177 of nitrogen from the ocean is assumed to be denitrification (NO_3^- reduction to N_2), which occurs
178 in suboxic-to-anoxic parts of the water column (here defined as <4.5 μM O_2; Keeling et al., 2009)
179 and in anoxic sedimentary porewaters. We did not separately parameterize the anammox
180 pathway (NH_4^+ oxidation to N_2 using NO_2^-) because the isotopic effect is similar to canonical
181 denitrification and thus a changing balance between anammox and canonical denitrification is
182 unlikely to affect the nitrogen isotope mass balance of the ocean (Devol, 2015).
183 We first calibrated our model to reproduce the isotopic mass balance of the modern ocean
184 (Devol, 2015). Then we adjusted the balance of water column and sedimentary denitrification as
185 a function of anoxia in the ocean. The isotopic composition of export production was calculated
186 for two end-member scenarios: (1) a closed system where nitrate is irreversibly transformed into
187 either N_2 (via denitrification) or biomass (via assimilation) (*i.e.* resulting in progressive isotopic
188 distillation of the residual pool at higher yields), and (2) an open system at steady state (*i.e.*
189 resulting in isotopic offsets between products and reactants that are nearly identical to the
190 fractionation factor) (cf. Hayes, 2004). Because the residence time of nitrogen in the modern
191 ocean is ~3 kyrs (Brandes and Devol, 2002), nitrogen is moderately well-mixed in the modern
192 open ocean, and thus nitrogen isotope mass balance should generally follow open-system
193 dynamics (as is assumed for carbon isotope mass balance; Hayes, 2004; Schidlowski, 2001).
194 However, in modern basins with very high rates of water column denitrification, the isotopic

distillation of residual NO_3^- can locally approach closed system dynamics, causing nitrogen isotope ratios in certain regions of the modern ocean to become substantially elevated above global mean values (Tesdal et al., 2013). In the low-oxygen Precambrian ocean, closed-system behavior of nitrogen isotopes may have been more prevalent, particularly prior to the GOE. Thus, we present both calculations, noting that the open-system scenario more accurately captures the global average value for marine sediments with predominantly oxic environments, while local environments can be susceptible to closed system dynamics. A full description of all parameterizations and equations can be found in the Supplementary Materials.

4. Results

4.1 Isotopic results

All of the studied units consistently show bulk-rock $\delta^{15}N$ values (Fig. 2; Table S1) that are elevated above the range expected from nitrogen fixation alone (-2‰ to +1‰; Zhang et al., 2014). The mean $\delta^{15}N_{bulk}$ value of all units analyzed is +4.8 ± 1.4‰ (1σ), which closely resembles the nitrogen isotope composition of modern marine sediments (mode +4‰ to +6‰; Tesdal et al., 2013). Within individual units, $\delta^{15}N_{bulk}$ values are fairly consistent over several meters in stratigraphy, with an average per-unit standard deviation of 0.6‰ (ranging from 0.2‰ to 1.8‰). The full range of $\delta^{15}N_{bulk}$ values in the samples analyzed in this study is +1.1‰ to +7.7‰, which largely overlaps the range seen in modern marine sediments (Tesdal et al., 2013). Notably, we find no evidence of extremely enriched $\delta^{15}N_{bulk}$ values (>+10‰) in any of the units studied here (Fig. 2), which stands in contrast to the data from Paleoproterozoic shales of the Aravalli Supergroup in India (Papineau et al., 2009).

Kerogen isolates were isotopically lighter than their corresponding bulk-rock values by an average of -2.5‰ (Fig. 3; Table S1). The isotopic offset increased as a function of metamorphic grade, with unmetamorphosed samples showing a small positive offset (+0.6‰; n = 4), while samples that reached prehnite-pumpellyite facies (-2.4‰; n = 6) and lower greenschist facies (-3.2‰; n = 20) showed a moderate negative offset (Fig. 3).

A LOWESS (LOcally WEighted Scatterplot Smoothing) curve was used to describe variability in the nitrogen isotope record across the GOE (details can be found in Supplementary Materials). Bulk-rock nitrogen isotope data from Precambrian marine sedimentary rocks were compiled from the literature by updating a published database (Stüeken et al., 2016). All published data from units spanning 3.3 to 1.3 Ga were included in the LOWESS calculations. The mean $\delta^{15}N$ value of the LOWESS curve is +3.6 ± 1.2‰ (1σ). The curve shows a secular trend across the GOE, with $\delta^{15}N$ values rising in the late Archean, reaching a maximum just prior to the GOE, stabilizing across much of the Paleoproterozoic, and slightly decreasing in the Mesoproterozoic (Fig. 9).

The mean $\delta^{13}C_{org}$ value of all samples in our dataset is -32.5 ± 7.3‰ (1σ). As with $\delta^{15}N$, $\delta^{13}C_{org}$ values for individual units are fairly consistent, with an average per-unit standard deviation of 1.8‰ (ranging from 0.2‰ to 3.9‰). Most studied units contain samples with $\delta^{13}C_{org}$ values that are more negative than the range typically generated by marine phytoplankton (-26‰ ± 7‰; Schidlowski, 2001), which might reflect heterotrophic activity, including methanogenesis, occurring in predominantly anoxic sediments, and methanotrophy either at the sediment-water interface or throughout the overlying water column utilizing dissolved oxidants (e.g. Bekker et al., 2008; Luo et al., 2014). A notable exception is an increase in $\delta^{13}C_{org}$ values seen in units deposited during the ca. 2.22-2.06 Ga Lomagundi carbon isotope excursion (Fig. 2), with $\delta^{13}C_{org}$

239 values rising to -22.6 ± 2.2‰ (1σ) in the Wewe Slate and -25.7 ± 3.0‰ (1σ) in the Sengoma
240 Argillite Formation (Bekker et al., 2008).
241
242 *4.2 Model outputs*
243 The box model-estimated mean $\delta^{15}N$ value for modern marine sediments (assuming open-
244 system dynamics) is +4.5‰, with a confidence interval of +2.6‰ to +7.3‰ based on
245 uncertainties in fractionation factors for nitrogen fixation and water column denitrification. The
246 closed system approach yields similar results (mean = +5.5‰, range of +3.5‰ to +8.5‰). Both
247 approaches thus accurately capture the average composition of modern marine sediments
248 (mode +4-6‰ ± 2.5‰; Tesdal et al., 2013).
249 As the relative proportion of suboxic-to-anoxic ocean water increases beyond modern
250 values and approaches 100% (i.e. p_{an+sub} approaches 100), sedimentary $\delta^{15}N$ values first increase
251 due to enhanced water column denitrification, but ultimately decline toward the "N_2-fixation
252 window" (-2‰ to +1‰) in strongly anoxic oceans (Fig. 8) because the rate of nitrogen removal is
253 so rapid (and nearly quantitative) that nitrogen-fixing rather than nitrate-assimilating organisms
254 dominate the nitrogen isotope mass-balance (cf. Fennel et al., 2005). In the closed system model,
255 values do not return to the "N_2-fixation window" even in fully anoxic oceans (f_{an+sub} = 100),
256 because the extremely fractionated nitrate associated with a totally closed system would still
257 drive sedimentary $\delta^{15}N$ values to become positive even with a minimal biomass contribution from
258 nitrate-assimilating organisms. However, such extreme fractionations are unlikely to have
259 occurred, since the ocean cannot be a totally closed system (*i.e.* nitrogen is continually being
260 fixed into biomass and made bioavailable through remineralization and nitrification). Reality for

261 the full range of ocean redox states thus lies somewhere between the two endmembers captured
262 by the separate calculations.
263
264 **5. Discussion**
265 *5.1 Preservation of primary isotopic signals*
266 Before using nitrogen isotopes in ancient marine sedimentary rocks to reconstruct
267 paleoenvironmental conditions, it must be demonstrated on a case-by-case basis that the
268 observed isotopic signatures indeed reflect the primary cycling of nitrogen in the ocean at the
269 time of deposition (Ader et al., 2016). This screening draws first from consideration of nitrogen
270 cycling in the modern ocean. The nitrogen isotopic composition of modern marine sediments
271 faithfully records the $\delta^{15}N$ value of biomass exported from the photic zone (Altabet and Francois,
272 1994), which is an admixture of nitrogen-fixing and nitrogen-assimilating organisms. Planktonic
273 biomass in the modern ocean has an average molar C/N ratio of ~7 (Redfield, 1934), and the
274 remineralization of biomass in the water-column and sediments can increase the C/N values
275 preserved in marine sediments. The C/N values of our samples predominantly fall between 5
276 and 100 (Fig. 4), which is consistent with moderate diagenetic reworking of primary biomass.
277 The Timeball Hill Formation has several samples with C/N values <5 (Fig. 4), which suggests
278 either (a) trapping of nitrogen in clay minerals during diagenesis, while carbon was oxidized and
279 lost from the system, or (b) post-depositional introduction of non-primary nitrogen (perhaps via
280 hydrothermal fluids). As discussed below, the fact that kerogen extracts from these samples
281 show expected isotopic offsets is consistent with a primary biomass origin for the nitrogen in
282 these samples, as was suggested by Luo et al. (2018).

283 Diagenesis can modify the $\delta^{15}N$ values of organic matter in marine sediments, but this effect
284 is typically much smaller than the fractionations imparted during nitrogen cycling in the water
285 column. In oxic sediments, the remineralization of organic-bound nitrogen can leave residual
286 biomass isotopically heavier by 1.4-2.3‰ (Lehmann et al., 2002; Möbius, 2013). However, the
287 effect is smaller under anoxic conditions (Lehmann et al., 2002), which likely prevailed in
288 Precambrian marine sedimentary environments. Thus, while the precise contribution of
289 diagenesis is difficult to assess, the isotopic effect of diagenesis on the $\delta^{15}N$ values was probably
290 minor (<1‰) compared to the magnitude of the isotopic enrichment (>>1‰) seen in these
291 samples.

292 After diagenesis, nitrogen isotope ratios can be further modified during metamorphism. This
293 involves two types of isotopic effects: isotopic partitioning between kerogen- and mineral-bound
294 nitrogen within the bulk rock (Stüeken et al., 2017) and loss of nitrogen out of the bulk rock
295 (Bebout and Fogel, 1992; Haendel et al., 1986). While the isotopic partitioning between nitrogen
296 phases within a bulk-rock sample can be significant (3-4‰) at low metamorphic grades (Stüeken
297 et al., 2017), the effect of nitrogen loss on bulk-rock $\delta^{15}N$ values is typically small in units that
298 have remained below greenschist-facies metamorphism (<1‰) or even within greenschist facies
299 (1-2‰; Rivera et al., 2015). The finding that $\delta^{15}N_{ker}$ values are systematically depleted (on average
300 by -2.5‰) relative to corresponding $\delta^{15}N_{bulk}$ values in this dataset is consistent with previous
301 studies of metamorphic effects on nitrogen isotope partitioning (Stüeken et al., 2017).
302 Furthermore, the increase in isotopic offset from near-zero in unmetamorphosed samples to
303 ~3‰ in lower greenschist facies samples (Fig. 3) is in good agreement with a systematic survey
304 of metamorphic effects on sedimentary $\delta^{15}N$ values (Stüeken et al., 2017). Thus, we follow

Stüeken et al. (2017) in taking $\delta^{15}N_{bulk}$ values as a more robust indicator of primary $\delta^{15}N$ values in these samples.

In cases where metamorphism has significantly altered bulk-rock nitrogen isotope ratios, it has been shown that progressive metamorphism causes preferential loss of nitrogen relative to carbon, and of ^{14}N relative to ^{15}N (Bebout and Fogel, 1992). Thus, a positive correlation between $\delta^{15}N_{bulk}$ and C/N ratios can be indicative of metamorphic alteration of bulk-rock nitrogen isotope ratios, and a positive correlation between $\delta^{15}N_{bulk}$ and $\delta^{13}C_{org}$ would suggest that both nitrogen and carbon isotopes were affected by metamorphism. There are no such positive correlations observed across our entire dataset (Fig. 5) or within individual units (Figs. S1 and S2), including those that reached greenschist facies metamorphism. The effect of metamorphism on the bulk-rock nitrogen and organic carbon isotope ratios in these samples was therefore probably minor, meaning that the trends in nitrogen and carbon isotopes seen across the GOE are primary isotopic signals indicative of environmental conditions at the time of deposition.

5.2 Interpretation of isotopic data

5.2.1 Mechanisms for generating positive $\delta^{15}N$ values

There are multiple ways to generate positive $\delta^{15}N$ values in ancient marine sedimentary rocks (see Ader et al., 2016; Stüeken et al., 2016). These mechanisms all pertain to the cycling of nitrogen after biological N_2 fixation, which imparts only a small fractionation under most conditions (-2‰ to +1‰; Zhang et al., 2014). Under conditions of replete dissolved Fe supply this fractionation can be slightly larger, generating biomass that is depleted by as much as -4‰ relative to atmospheric nitrogen (Zerkle et al., 2008). However, the lack of fairly negative $\delta^{15}N$

values in the Precambrian rock record – even in environments that are thought to have been ferruginous and dominated by N_2 fixation – suggests that these extreme conditions were not representative of global nitrogen cycling (Koehler et al., 2017; Stüeken, 2013; Stüeken et al., 2015).

As discussed in Section 5.1, the release of nitrogen during remineralization of organic matter imparts a negligible fractionation, making it unlikely to explain an isotopic enrichment of several permil. However, the re-assimilation of ammonium (NH_4^+) generated during remineralization can impart a large isotopic fractionation (up to -27‰) if the process is non-quantitative, with biomass becoming isotopically light (Hoch et al., 1992). Such a mechanism has been proposed to explain the very large spread of $\delta^{15}N$ values seen in shales of the late Paleoproterozoic Aravalli Supergroup (Papineau et al., 2009). This mechanism would require that non-quantitative NH_4^+ assimilation created a pool of isotopically light biomass and drove the isotopic composition of residual NH_4^+ isotopically heavy. The transport of the heavy nitrogen to another site and subsequent quantitative assimilation could plausibly generate elevated $\delta^{15}N$ values in marine sediments. However, the absence of isotopically light nitrogen in the nine units studied here makes this explanation seem unlikely. Furthermore, even in modern redox-stratified marine basins, such as the Black Sea, the accumulation of appreciable dissolved NH_4^+ does not correlate with isotopic evidence of partial assimilation (e.g. Fulton et al., 2012). Sediments underlying these modern anoxic waters have $\delta^{15}N$ values near 0‰, suggestive of nitrogen fixation in the photic zone followed by quantitative uptake of liberated NH_4^+. This can be attributed to the fact that nitrogen is the limiting nutrient in the ocean on short, Ka-timescales (Tyrrell, 1999), and thus uptake of bioavailable nitrogen in the photic zone is typically quantitative.

While nitrogen uptake into biomass tends to have no net isotopic effect, partial removal of bioavailable nitrogen from the ocean through redox processes can result in significant isotopic fractionations. One such pathway is the nitrification of NH_4^+ into NO_3^-, which – if non-quantitative – can create a NO_3^- pool that is isotopically light and leave a residual, heavy pool of NH_4^+ (Casciotti et al., 2003). The resulting biomass could become isotopically heavy if organisms quantitatively assimilate the heavy NH_4^+, while the light NO_3^- is quantitatively removed via denitrification to the atmosphere (Thomazo et al., 2011). However, it is unlikely that this sort of system would have been stable on geological timescales. Today, partial nitrification is only observed in regions of the modern ocean where seasonal redox-stratification occurs (e.g. Granger et al., 2011). This is because nitrification is rapid, and can even proceed at nanomolar levels of dissolved oxygen (e.g. Kalvelage et al., 2011). Furthermore, the same conditions that would favor non-quantitative nitrification (seasonally variable redox-stratification) might be inimical to quantitative denitrification, as the latter process is not as rapid, and rarely goes to completion in the open ocean (Devol, 2015).

Another explanation for isotopic enrichment in marine settings is non-quantitative denitrification occurring in suboxic regions of the open ocean. This process imparts a large isotopic fractionation (-10 to -30‰; Devol, 2015; Kritee et al., 2012), causing residual dissolved NO_3^- to become isotopically heavy ($\delta^{15}N > 0‰$). Importantly, denitrification occurring in sedimentary porewaters nearly goes to completion, resulting in a flux of isotopically heavy nitrogen from the ocean back into the atmosphere, counterbalancing the isotopically light flux from suboxic waters. The quantitative assimilation of the residual heavy NO_3^- then records the net isotopic distillation of the reservoir imparted by denitrification, which ultimately gets

371 preserved in marine sediments. This mechanism is thought to control the isotopic mass balance
372 of the modern ocean system (Devol, 2015), causing the $\delta^{15}N$ values of most modern marine
373 sediments to fall between +4‰ and +6‰ (Tesdal et al., 2013).

374 Considering all possible mechanisms listed above, the positive $\delta^{15}N$ values seen in the
375 Paleoproterozoic units studied here are most compellingly explained by similar processes to
376 those operating in the modern ocean: rapid nitrification, non-quantitative denitrification in
377 suboxic regions of the water column, and quantitative assimilation of residual NO_3^- in the photic
378 zone. In other words, our nitrogen isotope data suggest that an aerobic nitrogen cycle persisted
379 across continental shelves between about 2.44 and 1.85 Ga.

380

381 *5.2.2 Aerobic nitrogen cycling in the early Paleoproterozoic*

382 While transient excursions to elevated $\delta^{15}N$ values – indicative of local aerobic nitrogen
383 cycling – have been observed in Neoarchean shales (Garvin et al., 2009; Koehler et al., in press),
384 it remains unclear to what extent these settings are representative of global redox conditions at
385 that time. The large isotopic variability seen in some Neoarchean facies is consistent with a small
386 NO_3^- reservoir (Garvin et al., 2009; Koehler et al., in press), which could promote substantial inter-
387 basinal variability and closed-system dynamics (discussed further in Section 5.3). In contrast, the
388 more stable stratigraphic $\delta^{15}N$ profiles of the Paleoproterozoic (Fig. 5) may reflect growth of the
389 NO_3^- reservoir, with the ocean residence time of NO_3^- becoming sufficiently long that relatively
390 rapid and large-magnitude isotopic excursions are not seen within continuous lithostratigraphic
391 units. This was first suggested by Zerkle et al. (2017), who found evidence of aerobic nitrogen
392 cycling in the early stages of the GOE in the 2.32 Ga Lower Timeball Hill Formation of the Pretoria

393 Group in South Africa, and further confirmed by the findings of another recent study of multiple
394 drill cores in the Pretoria Group (Luo et al., 2018). Our dataset corroborates those findings,
395 showing instances of elevated $\delta^{15}N$ values in the Upper Timeball Hill Formation. Additionally, we
396 find that shales of the ca. 2.44 Ga Turee Creek Group in Western Australia, which were deposited
397 shortly before the onset of the GOE, have $\delta^{15}N$ values (ranging from +2‰ to +3‰) that are
398 consistent with a minor, but persistent, contribution of aerobic nitrogen cycling to the isotopic
399 composition of preserved biomass. However, because diagenetic and metamorphic overprinting
400 could have potentially contributed a post-depositional enrichment of $\delta^{15}N_{bulk}$ values by ~1-2‰,
401 it is difficult to use the Turee Creek data to precisely gauge the extent of aerobic nitrogen cycling
402 immediately prior to the GOE.

403 The state of the nitrogen cycle appears to have been fairly stable across the GOE and the
404 proposed "oxygen overshoot" during the Lomagundi carbon isotope excursion (ca. 2.22-2.06 Ga;
405 Bekker and Holland, 2012). Even in the aftermath of the GOE (i.e. after ca. 2.06 Ga), when sulfur
406 and selenium isotope records point to a contraction of oxygenated seawater (Planavsky et al.,
407 2012; Scott et al., 2014; Kipp et al., 2017), nitrogen isotopes continue to record aerobic nitrogen
408 cycling in the surface ocean (Fig. 7). This is unlikely to be an artifact of poor age constraints and
409 low sample density – many of the nitrogen isotope data are from the same units that were used
410 to argue for waxing and waning marine oxygen levels across the GOE based on molybdenum
411 (Scott et al., 2008) and uranium (Partin et al., 2013) enrichments, multiple sulfur isotopes (Scott
412 et al., 2014), and selenium enrichments and isotope ratios (Kipp et al., 2017). Instead, the
413 differential response of these redox proxies may be indicative of the mechanism by which the

414 Earth transitioned from the “oxygen overshoot” interval to the apparently oxygen-limited mid-
415 Proterozoic.

416 The record of sedimentary enrichments of redox-sensitive elements is influenced by both
417 the rate of continental oxidative weathering, which supplies them to the ocean, and the areal
418 extent of anoxic and euxinic marine sediments, which efficiently scavenge redox-sensitive
419 elements from the water column. The sharp peak in redox-sensitive trace element enrichments
420 between 2.32 Ga and 2.06 Ga is thus suggestive of both vigorous oxidative weathering and an
421 expansion of at least mildly oxygenated waters at the expense of anoxic and euxinic settings
422 (Partin et al., 2013; Kipp et al., 2017). The size of the marine sulfate reservoir is sensitive to the
423 same conditions, and correspondingly shows a similar trend, as inferred from both carbonate-
424 associated sulfate (Planavsky et al., 2012) and multiple sulfur isotope data from sedimentary
425 sulfides (Scott et al., 2014). In contrast, sedimentary nitrogen isotope ratios reflect the balance
426 between nitrogen fixation and assimilation of dissolved NO_3^- (the isotopic composition of the
427 latter being predominantly set by rates of denitrification) in the part of the water column where
428 primary productivity is the highest, *i.e.* the photic zone. Unlike sulfur and trace metals, NO_3^- is
429 largely produced within the ocean via nitrification and thus to a first order is independent from
430 oxidative weathering. The persistence of isotopic evidence for NO_3^- uptake after the proposed
431 “oxygen overshoot” interval therefore suggests that the photic zone on continental shelves
432 remained at least mildly oxygenated in the aftermath of the GOE, while the areal extent of anoxic
433 marine sediments increased.

434 This aerobic state of the nitrogen cycle has not persisted uninterrupted since the GOE. In
435 the Mesoproterozoic, basinal gradients in $\delta^{15}N$ values have been observed, with near-shore facies

436 recording aerobic nitrogen cycling, while offshore facies reflect quantitative assimilation and
437 nitrogen fixation (Stüeken, 2013; Koehler et al., 2017). Our dataset samples only relatively deep-
438 water environments, so we cannot speak to basinal $\delta^{15}N$ gradients within any of the units studied
439 here. However, the persistence of elevated $\delta^{15}N$ values in these settings during and after the GOE
440 demonstrates that aerobic nitrogen cycling prevailed even on the outer shelf. With the available
441 data we are unable to precisely constrain the time at which basinal gradients became
442 representative of the global nitrogen cycle. However, some insight into this matter is offered by
443 the youngest unit in our dataset, the ca. 1.85 Ga Menihek Formation of the Superior Craton in
444 Canada. The positive $\delta^{15}N$ values (+3.9 to +5.0‰) and small isotopic variability (1σ = 0.3‰) in this
445 unit are both consistent with a significant contribution of aerobic nitrogen cycling and a large
446 bioavailable NO_3^- reservoir in offshore environments in this basin. Thus, this unit might provide a
447 maximum age for the transition to the basinal stratification observed in the Mesoproterozoic
448 nitrogen isotope record.
449
450 *5.3 Quantifying the relationship between ocean oxygenation and nitrogen cycling*
451 While a qualitative interpretation of this dataset yields a compelling story about the
452 oxygenation of the surface ocean in the early Paleoproterozoic, more information can be
453 gleaned by considering these data in a quantitative framework. Our model outputs (Fig. 8) show
454 that under pervasive anoxia ($p_{an\text{-}sub}$ approaching 100%), sedimentary $\delta^{15}N$ values approach the
455 "N_2 fixation window" (-2‰ to +1‰), which indicates that assimilation of NO_3^- into biomass
456 becomes negligible due to increasing denitrification rates. Under these conditions, the majority
457 of marine biomass is comprised of either N_2-fixing organisms or NH_4^+ assimilating organisms

458 (which were not explicitly tracked in the model). In either case, NO_3^-, which is the preferred
459 nitrogenous compound utilized by eukaryotes in the modern ocean (Karl et al., 2001), is rapidly
460 removed via water column denitrification in strongly anoxic oceans, preventing NO_3^-
461 assimilators from contributing substantially to sedimentary export production (cf. Fennel et al.,
462 2005).

463 These results suggest that the persistence of a stable, isotopically recordable NO_3^- reservoir
464 requires perhaps as much as ~90% of the surface ocean to be at least mildly oxygenated (Fig. 8).
465 Precisely what concentration of dissolved O_2 defines "mildly oxygenated" is unresolved by this
466 model; for the purpose of this discussion, we are referring to the O_2 level at which nitrification
467 outpaces denitrification, thereby allowing the accumulation of a bioavailable nitrate reservoir.
468 In our model scenarios we dictated that the switch to denitrifying conditions occurs when
469 dissolved O_2 falls below 4.5 μM (meaning that higher levels would constitute "mildly
470 oxygenated" waters) because the majority of water column denitrification occurs in these
471 settings in the modern ocean (Codispoti et al., 2001; Keeling et al., 2009; Paulmier and Ruiz-
472 Pino, 2009). However, it is known that denitrification can occur at dissolved O_2 levels of >20 μM
473 (Kalvelage et al., 2011) and previous modeling has suggested that denitrification outpaces
474 nitrification until dissolved O_2 exceeds 11 μM (Fennel et al., 2005). Regardless of precisely where
475 this threshold lies, the persistence of aerobic nitrogen cycling across much of the
476 Paleoproterozoic suggests that the threshold was exceeded in the surface waters of most basins
477 for a few hundred million years following the GOE.

478 This is a particularly important consideration when addressing the meaning of elevated $\delta^{15}N$
479 values in Neoarchean versus Paleoproterozoic marine sedimentary rocks. In studies of

480 Neoarchean units, large deviations from the "N_2 fixation window" towards elevated values have
481 been interpreted as indicating transient oxygenation in the water column prior to the GOE
482 (Garvin et al., 2009; Koehler et al., in press). The Neoarchean basins in which these trends were
483 observed most likely conformed to closed system dynamics rather than the open-system
484 dynamics that characterize nitrogen isotope mass balance in the modern ocean, because the
485 NO_3^- was sourced locally in the upper water column and was unlikely to become well-mixed in
486 such a strongly anoxic ocean. With this being the case, further studies that increase spatial
487 resolution of the nitrogen isotope record in the potentially heterogeneous Neoarchean ocean
488 could help determine whether the positive $\delta^{15}N$ values in those strata record local or global
489 redox fluctuations.
490
491 *5.4 Implications for primary productivity and the emergence of eukaryotic ecosystems*
492 Before the GOE, it is thought that a scarcity of phosphorus restricted rates of primary
493 productivity (Bekker and Holland, 2012; Kipp and Stüeken, 2017; Reinhard et al., 2016). The lack
494 of sufficient oxidizing power may have inhibited the recycling of organic-bound phosphorus
495 within the ocean until marine dissolved oxygen and sulfate levels rose in the Paleoproterozoic
496 (Planavsky et al., 2012; Scott et al., 2014), implying that the total rate of carbon recycling and
497 net primary productivity could have increased in tandem with the oxygenation of the Earth's
498 surface environments (cf. Bekker and Holland, 2012). It is conceivable that an increase in
499 phosphorus availability during the GOE (cf. Bekker and Holland, 2012) could have caused
500 nitrogen to become the limiting nutrient in the marine environment. However, the data
501 presented here, as well as those presented in previous studies of nitrogen isotopes in

Paleoproterozoic marine sedimentary rocks (Godfrey et al., 2013; Kump et al., 2011; Luo et al., 2018; Papineau et al., 2009; Zerkle et al., 2017), show no evidence of persistent nitrogen limitation on geological timescales after the onset of the GOE. Quite to the contrary, the persistence of elevated nitrogen isotope ratios in Paleoproterozoic shales suggests that fixed nitrogen was sufficiently available to fuel primary production (discussed in Section 5.2.1). Still, while nitrogen was likely not limiting, it is not entirely clear whether it was phosphorus, trace metals, or some other factor that controlled the rate of primary productivity during the Lomagundi carbon isotope excursion and associated "oxygen overshoot" interval, which is thought to have been a time of extreme organic carbon burial (Bekker and Holland, 2012; Karhu and Holland, 1996).

A further question is whether these more productive, nitrate-fueled ecosystems contained eukaryotic organisms. Considerable controversy surrounds the oldest evidence of eukaryotes; it is generally accepted that the eukaryotic lineage had emerged by ca. 1.7 Ga (see Javaux and Lepot, 2018), though arguments for an earlier arrival of eukaryotes are not lacking (e.g. Bengtson et al., 2017; El Albani et al., 2010). Notably, a recent genomic effort to resolve the origin of sterol biosynthesis has suggested that this metabolic capacity – a hallmark of eukaryotic organisms – evolved nearly contemporaneously with the onset of the GOE (Gold et al., 2017). However, the record of organic biomarkers in Proterozoic sedimentary successions implies that eukaryotes were not significant contributors to bulk organic matter until the late Neoproterozoic (Brocks et al., 2017). While efforts to confidently constrain when the eukaryotes first evolved and reached abundance in the sedimentary record will carry on, geochemical constraints will be critical to

523 answering fundamental questions about the interplay between environmental changes and
524 biological responses.

525 The data presented here have two implications for early eukaryotic evolution. First, the
526 prevalence of elevated $\delta^{15}N$ values in the early Paleoproterozoic (Figs. 7, 9) is direct evidence of
527 abundant NO_3^- assimilating organisms. Whether a substantial portion of this biomass was
528 comprised of eukaryotes is unclear from the nitrogen isotope data alone, but this trend in
529 nitrogen isotopes confirms that NO_3^- was sufficiently bioavailable across continental shelves to
530 alleviate any fixed-nitrogen limitation on eukaryotic proliferation at this time (Fig. 9). Second,
531 the magnitude of nitrogen isotope enrichment and consistency of values, when viewed in the
532 context of our model outputs, imply that much of the photic zone overlying continental shelves
533 was at least mildly oxygenated for hundreds of millions of years in the Paleoproterozoic. Thus,
534 if they had already evolved, eukaryotes with oxygen-requiring metabolic processes should have
535 been able to persist in the upper part of the water column without severe oxygen-limitation.
536 Still, it remains plausible that periodic incursions of anoxic waters and redox fluctuations at low
537 dissolved O_2 levels could have restricted the proliferation and diversification of eukaryotes at
538 this time (cf. Johnston et al., 2012). In any case, the data presented here allow for an earlier
539 emergence of eukaryotes than is deemed likely under recent interpretations of the fossil and
540 biomarker records (Fig. 9).

541

542 **6. Conclusion**

543 We have presented new nitrogen isotope data spanning the Paleoproterozoic Era that
544 document persistent aerobic nitrogen cycling on continental shelves from ca. 2.44 to 1.85 Ga.

545 The observation that nitrogen isotope ratios remain elevated when trace metal and sulfur-based
546 proxies point to a decrease in the extent of oxic settings following the ca. 2.32-2.06 Ga "oxygen
547 overshoot" may derive from the fact that the latter proxies are sensitive to redox conditions at
548 the sediment-water interface, while nitrogen isotope values record redox conditions in the photic
549 zone. When viewed in light of our model outputs, these data implicate oxygenated surface
550 seawater and substantial bioavailable NO_3^- lasting from the onset of the GOE until at least ca.
551 1.85 Ga. This may suggest that the upper ocean was already hospitable to eukaryotic organisms
552 hundreds of millions of years before the fossil record firmly indicates their presence.
553

554 **Acknowledgements**

555 We thank Andy Schauer and the UW IsoLab for technical support. MAK acknowledges support
556 from NSF Graduate Research Fellowship DGE-1256082. AB acknowledges funding from NSERC
557 Discovery and Accelerator grants. Funding for isotopic analyses was provided by the UW
558 Department of Earth & Space Sciences to MAK and by NASA Exobiology grant NNX16AI37G to RB.
559 We thank Vincent Busigny and one anonymous reviewer for comments that substantially
560 improved this work, as well as Derek Vance for editorial handling.
561

References

Ader, M., Thomazo, C., Sansjofre, P., Busigny, V., Papineau, D., Laffont, R., Cartigny, P., Halverson, G.P., 2016. Interpretation of the nitrogen isotopic composition of Precambrian sedimentary rocks: Assumptions and perspectives. Chem. Geol. 429, 93–110.

Altabet, M.A., Francois, R., 1994. Sedimentary nitrogen isotopic ratio as a recorder for surface ocean nitrate utilization. Glob. Biogeochem. Cycles 8, 103–116.

Bebout, G.E., Fogel, M.L., 1992. Nitrogen-isotope compositions of metasedimentary rocks in the Catalina Schist, California: implications for metamorphic devolatilization history. Geochim. Cosmochim. Acta 56, 2839–2849.

Bekker, A., Holland, H.D., 2012. Oxygen overshoot and recovery during the early Paleoproterozoic. Earth Planet. Sci. Lett. 317, 295–304. https://doi.org/10.1016/j.epsl.2011.12.012

Bekker, A., Holland, H.D., Wang, P.-L., Rumble, D., Stein, H.J., Hannah, J.L., Coetzee, L.L., Beukes, N.J., 2004. Dating the rise of atmospheric oxygen. Nature 427, 117–120.

Bekker, A., Holmden, C., Beukes, N.J., Kenig, F., Eglinton, B., Patterson, W.P., 2008. Fractionation between inorganic and organic carbon during the Lomagundi (2.22–2.1 Ga) carbon isotope excursion. Earth Planet. Sci. Lett. 271, 278–291.

Bengtson, S., Rasmussen, B., Ivarsson, M., Muhling, J., Broman, C., Marone, F., Stampanoni, M., Bekker, A., 2017. Fungus-like mycelial fossils in 2.4-billion-year-old vesicular basalt. Nat. Ecol. Evol. 1, 0141.

Beukes, N.J., Dorland, H., Gutzmer, J., Nedachi, M., Ohmoto, H., 2002. Tropical laterites, life on land, and the history of atmospheric oxygen in the Paleoproterozoic. Geology 30, 491–494.

Brandes, J.A., Devol, A.H., 2002. A global marine-fixed nitrogen isotopic budget: Implications for Holocene nitrogen cycling. Glob. Biogeochem. Cycles 16.

Brocks, J.J., Jarrett, A.J., Sirantoine, E., Hallmann, C., Hoshino, Y., Liyanage, T., 2017. The rise of algae in Cryogenian oceans and the emergence of animals. Nature 548, 578.

Casciotti, K.L., Sigman, D.M., Ward, B.B., 2003. Linking diversity and stable isotope fractionation in ammonia-oxidizing bacteria. Geomicrobiol. J. 20, 335–353.

Codispoti, L.A., Brandes, J.A., Christensen, J.P., Devol, A.H., Naqvi, S.W.A., Paerl, H.W., Yoshinari, T., 2001. The oceanic fixed nitrogen and nitrous oxide budgets: Moving targets as we enter the anthropocene? Sci. Mar. 65, 85–105.

Devol, A.H., 2015. Denitrification, anammox, and N2 production in marine sediments. Annu. Rev. Mar. Sci. 7, 403–423.

El Albani, A., Bengtson, S., Canfield, D.E., Bekker, A., Macchiarelli, R., Mazurier, A., Hammarlund, E.U., Boulvais, P., Dupuy, J.-J., Fontaine, C., Fürsich, F.T., Gauthier-Lafaye, F., Janvier, P., Javaux, E., Ossa, F.O., Pierson-Wickmann, A.-C., Riboulleau, A., Sardini, P., Vachard, D., Whitehouse, M., Meunier, A., 2010. Large colonial organisms with coordinated growth in oxygenated environments 2.1 Gyr ago. Nature 466, 100–104. https://doi.org/10.1038/nature09166

Farquhar, J., Bao, H.M., Thiemens, M., 2000. Atmospheric influence of Earth's earliest sulfur cycle. Science 289, 756–758. https://doi.org/10.1126/science.289.5480.756

Fennel, K., Follows, M., Falkowski, P.G., 2005. The co-evolution of the nitrogen, carbon and oxygen cycles in the Proterozoic ocean. Am. J. Sci. 305, 526–545.

Fulton, J.M., Arthur, M.A., Freeman, K.H., 2012. Black Sea nitrogen cycling and the preservation of phytoplankton δ15N signals during the Holocene. Glob. Biogeochem. Cycles 26.

Garvin, J., Buick, R., Anbar, A.D., Arnold, G.L., Kaufman, A.J., 2009. Isotopic evidence for an aerobic nitrogen cycle in the latest Archean. Science 323, 1045–1048.

Godfrey, L.V., Poulton, S.W., Bebout, G.E., Fralick, P.W., 2013. Stability of the nitrogen cycle during development of sulfidic water in the redox-stratified late Paleoproterozoic Ocean. Geology 41, 655–658.
Gold, D.A., Caron, A., Fournier, G.P., Summons, R.E., 2017. Paleoproterozoic sterol biosynthesis and the rise of oxygen. Nature 543, 420–423.
Granger, J., Prokopenko, M.G., Sigman, D.M., Mordy, C.W., Morse, Z.M., Morales, L.V., Sambrotto, R.N., Plessen, B., 2011. Coupled nitrification-denitrification in sediment of the eastern Bering Sea shelf leads to 15N enrichment of fixed N in shelf waters. J. Geophys. Res. Oceans 116.
Gumsley, A.P., Chamberlain, K.R., Bleeker, W., Söderlund, U., Kock, M.O. de, Larsson, E.R., Bekker, A., 2017. Timing and tempo of the Great Oxidation Event. Proc. Natl. Acad. Sci. 114, 1811–1816. https://doi.org/10.1073/pnas.1608824114
Haendel, D., Mühle, K., Nitzsche, H.-M., Stiehl, G., Wand, U., 1986. Isotopic variations of the fixed nitrogen in metamorphic rocks. Geochim. Cosmochim. Acta 50, 749–758.
Hardisty, D.S., Lu, Z., Bekker, A., Diamond, C.W., Gill, B.C., Jiang, G., Kah, L.C., Knoll, A.H., Loyd, S.J., Osburn, M.R., others, 2017. Perspectives on Proterozoic surface ocean redox from iodine contents in ancient and recent carbonate. Earth Planet. Sci. Lett. 463, 159–170.
Hayes, J.M., 2004. An introduction to isotopic calculations. Woods Hole Oceanogr. Inst. Woods Hole MA 2543.
Hoch, M.P., Fogel, M.L., Kirchman, D.L., 1992. Isotope fractionation associated with ammonium uptake by a marine bacterium. Limnol. Oceanogr. 37, 1447–1459.
Javaux, E., Lepot, K., 2018. The Paleoproterozoic fossil record: Implications for the evolution of the biosphere during Earth's middle-age. Earth-Sci. Rev. 176, 68–86.
Johnston, D.T., Poulton, S.W., Goldberg, T., Sergeev, V.N., Podkovyrov, V., Vorob'eva, N.G., Bekker, A., Knoll, A.H., 2012. Late Ediacaran redox stability and metazoan evolution. Earth Planet. Sci. Lett. 335, 25–35. https://doi.org/10.1016/j.epsl.2012.05.010
Kalvelage, T., Jensen, M.M., Contreras, S., Revsbech, N.P., Lam, P., Günter, M., LaRoche, J., Lavik, G., Kuypers, M.M.M., 2011. Oxygen Sensitivity of Anammox and Coupled N-Cycle Processes in Oxygen Minimum Zones. PLOS ONE 6, e29299. https://doi.org/10.1371/journal.pone.0029299
Karhu, J.A., Holland, H.D., 1996. Carbon isotopes and the rise of atmospheric oxygen. Geology 24, 867–870.
Karl, D.M., Bidigare, R.R., Letelier, R.M., 2001. Long-term changes in plankton community structure and productivity in the North Pacific Subtropical Gyre: The domain shift hypothesis. Deep Sea Res. Part II Top. Stud. Oceanogr. 48, 1449–1470.
Keeling, R.F., Körtzinger, A., Gruber, N., 2009. Ocean deoxygenation in a warming world.
Kipp, M.A., Stüeken, E.E., 2017. Biomass recycling and Earth's early phosphorus cycle. Sci. Adv. 3, eaao4795.
Kipp, M.A., Stüeken, E.E., Bekker, A., Buick, R., 2017. Selenium isotopes record extensive marine suboxia during the Great Oxidation Event. Proc. Natl. Acad. Sci. 114, 875–880. https://doi.org/10.1073/pnas.1615867114
Koehler, M.C., Buick, R., Kipp, M.A., Stüeken, E.E., Zaloumis, J., in press. Transient surface ocean oxygenation recorded in the ~2.66 Ga Jeerinah Formation, Australia. Proc. Natl. Acad. Sci.
Koehler, M.C., Stüeken, E.E., Kipp, M.A., Buick, R., Knoll, A.H., 2017. Spatial and temporal trends in Precambrian nitrogen cycling: A Mesoproterozoic offshore nitrate minimum. Geochim. Cosmochim. Acta 198, 315–337.
Kritee, K., Sigman, D.M., Granger, J., Ward, B.B., Jayakumar, A., Deutsch, C., 2012. Reduced isotope fractionation by denitrification under conditions relevant to the ocean. Geochim. Cosmochim. Acta 92, 243–259.

Kump, L.R., Junium, C., Arthur, M.A., Brasier, A., Fallick, A., Melezhik, V., Lepland, A., CČrne, A.E., Luo, G., 2011. Isotopic Evidence for Massive Oxidation of Organic Matter Following the Great Oxidation Event. Science 334, 1694–1696. https://doi.org/10.1126/science.1213999

Lehmann, M.F., Bernasconi, S.M., Barbieri, A., McKenzie, J.A., 2002. Preservation of organic matter and alteration of its carbon and nitrogen isotope composition during simulated and in situ early sedimentary diagenesis. Geochim. Cosmochim. Acta 66, 3573–3584.

Luo, G., Junium, C.K., Izon, G., Ono, S., Beukes, N.J., Algeo, T.J., Cui, Y., Xie, S., Summons, R.E., 2018. Nitrogen fixation sustained productivity in the wake of the Palaeoproterozoic Great Oxygenation Event. Nat. Commun. 9, 978.

Luo, G., Junium, C.K., Kump, L.R., Huang, J., Li, C., Feng, Q., Shi, X., Bai, X., Xie, S., 2014. Shallow stratification prevailed for 1700 to 1300 Ma ocean: Evidence from organic carbon isotopes in the North China Craton. Earth Planet. Sci. Lett. 400, 219–232.

Luo, G., Ono, S., Beukes, N.J., Wang, D.T., Xie, S., Summons, R.E., 2016. Rapid oxygenation of Earth's atmosphere 2.33 billion years ago. Sci. Adv. 2, e1600134. https://doi.org/10.1126/sciadv.1600134

Lyons, T.W., Reinhard, C.T., Planavsky, N.J., 2014. The rise of oxygen in Earth's early ocean and atmosphere. Nature 506, 307–315. https://doi.org/10.1038/nature13068

Möbius, J., 2013. Isotope fractionation during nitrogen remineralization (ammonification): Implications for nitrogen isotope biogeochemistry. Geochim. Cosmochim. Acta 105, 422–432.

Papineau, D., Purohit, R., Goldberg, T., Pi, D., Shields, G.A., Bhu, H., Steele, A., Fogel, M.L., 2009. High primary productivity and nitrogen cycling after the Paleoproterozoic phosphogenic event in the Aravalli Supergroup, India. Precambrian Res. 171, 37–56.

Partin, C.A., Bekker, A., Planavsky, N.J., Scott, C.T., Gill, B.C., Li, C., Podkovyrov, V., Maslov, A., Konhauser, K.O., Lalonde, S.V., Love, G.D., Poulton, S.W., Lyons, T.W., 2013. Large-scale fluctuations in Precambrian atmospheric and oceanic oxygen levels from the record of U in shales. Earth Planet. Sci. Lett. 369, 284–293. https://doi.org/10.1016/j.epsl.2013.03.031

Paulmier, A., Ruiz-Pino, D., 2009. Oxygen minimum zones (OMZs) in the modern ocean. Prog. Oceanogr. 80, 113–128.

Planavsky, N.J., Bekker, A., Hofmann, A., Owens, J.D., Lyons, T.W., 2012. Sulfur record of rising and falling marine oxygen and sulfate levels during the Lomagundi event. Proc. Natl. Acad. Sci. 109, 18300–18305. https://doi.org/10.1073/pnas.1120387109

Redfield, A.C., 1934. On the proportions of organic derivatives in sea water and their relation to the composition of plankton. James Johnstone Meml. Vol. 176–192.

Reinhard, C.T., Planavsky, N.J., Gill, B.C., Ozaki, K., Robbins, L.J., Lyons, T.W., Fischer, W.W., Wang, C., Cole, D.B., Konhauser, K.O., 2016. Evolution of the global phosphorus cycle. Nature 541, 386–389. https://doi.org/10.1038/nature20772

Rivera, K.T., Puckette, J., Quan, T.M., 2015. Evaluation of redox versus thermal maturity controls on δ 15 N in organic rich shales: a case study of the Woodford Shale, Anadarko Basin, Oklahoma, USA. Org. Geochem. 83, 127–139.

Schidlowski, M., 2001. Carbon isotopes as biogeochemical recorders of life over 3.8 Ga of Earth history: evolution of a concept. Precambrian Res. 106, 117–134.

Scott, C., Lyons, T.W., Bekker, A., Shen, Y., Poulton, S.W., Chu, X., Anbar, A.D., 2008. Tracing the stepwise oxygenation of the Proterozoic ocean. Nature 452, 456-U5. https://doi.org/10.1038/nature06811

Scott, C., Wing, B.A., Bekker, A., Planavsky, N.J., Medvedev, P., Bates, S.M., Yun, M., Lyons, T.W., 2014. Pyrite multiple-sulfur isotope evidence for rapid expansion and contraction of the early Paleoproterozoic seawater sulfate reservoir. Earth Planet. Sci. Lett. 389, 95–104. https://doi.org/10.1016/j.epsl.2013.12.010

Stüeken, E.E., 2013. A test of the nitrogen-limitation hypothesis for retarded eukaryote radiation: Nitrogen isotopes across a Mesoproterozoic basinal profile. Geochim. Cosmochim. Acta 120, 121–139. https://doi.org/10.1016/j.gca.2013.06.002

Stüeken, E.E., Buick, R., Guy, B.M., Koehler, M.C., 2015. Isotopic evidence for biological nitrogen fixation by molybdenum-nitrogenase from 3.2 Gyr. Nature 520, 666–669. https://doi.org/10.1038/nature14180

Stüeken, E.E., Kipp, M.A., Koehler, M.C., Buick, R., 2016. The evolution of Earth's biogeochemical nitrogen cycle. Earth-Sci. Rev. 160, 220–239.

Stüeken, E.E., Zaloumis, J., Meixnerová, J., Buick, R., 2017. Differential metamorphic effects on nitrogen isotopes in kerogen extracts and bulk rocks. Geochim. Cosmochim. Acta 217, 80–94. https://doi.org/10.1016/j.gca.2017.08.019

Tesdal, J.-E., Galbraith, E.D., Kienast, M., 2013. Nitrogen isotopes in bulk marine sediment: linking seafloor observations with subseafloor records. Biogeosciences 10, 101–118. https://doi.org/10.5194/bg-10-101-2013

Thomazo, C., Ader, M., Philippot, P., 2011. Extreme 15N-enrichments in 2.72-Gyr-old sediments: evidence for a turning point in the nitrogen cycle. Geobiology 9, 107–120.

Tyrrell, T., 1999. The relative influences of nitrogen and phosphorus on oceanic primary production. Nature 400, 525–531.

Zerkle, A.L., Junium, C.K., Canfield, D.E., House, C.H., 2008. Production of 15N-depleted biomass during cyanobacterial N2-fixation at high Fe concentrations. J. Geophys. Res. Biogeosciences 113, G03014. https://doi.org/10.1029/2007JG000651

Zerkle, A.L., Poulton, S.W., Newton, R.J., Mettam, C., Claire, M.W., Bekker, A., Junium, C.K., 2017. Onset of the aerobic nitrogen cycle during the Great Oxidation Event. Nature 543, 465–467.

Zhang, X., Sigman, D.M., Morel, F.M., Kraepiel, A.M., 2014. Nitrogen isotope fractionation by alternative nitrogenases and past ocean anoxia. Proc. Natl. Acad. Sci. 111, 4782–4787.

Figures

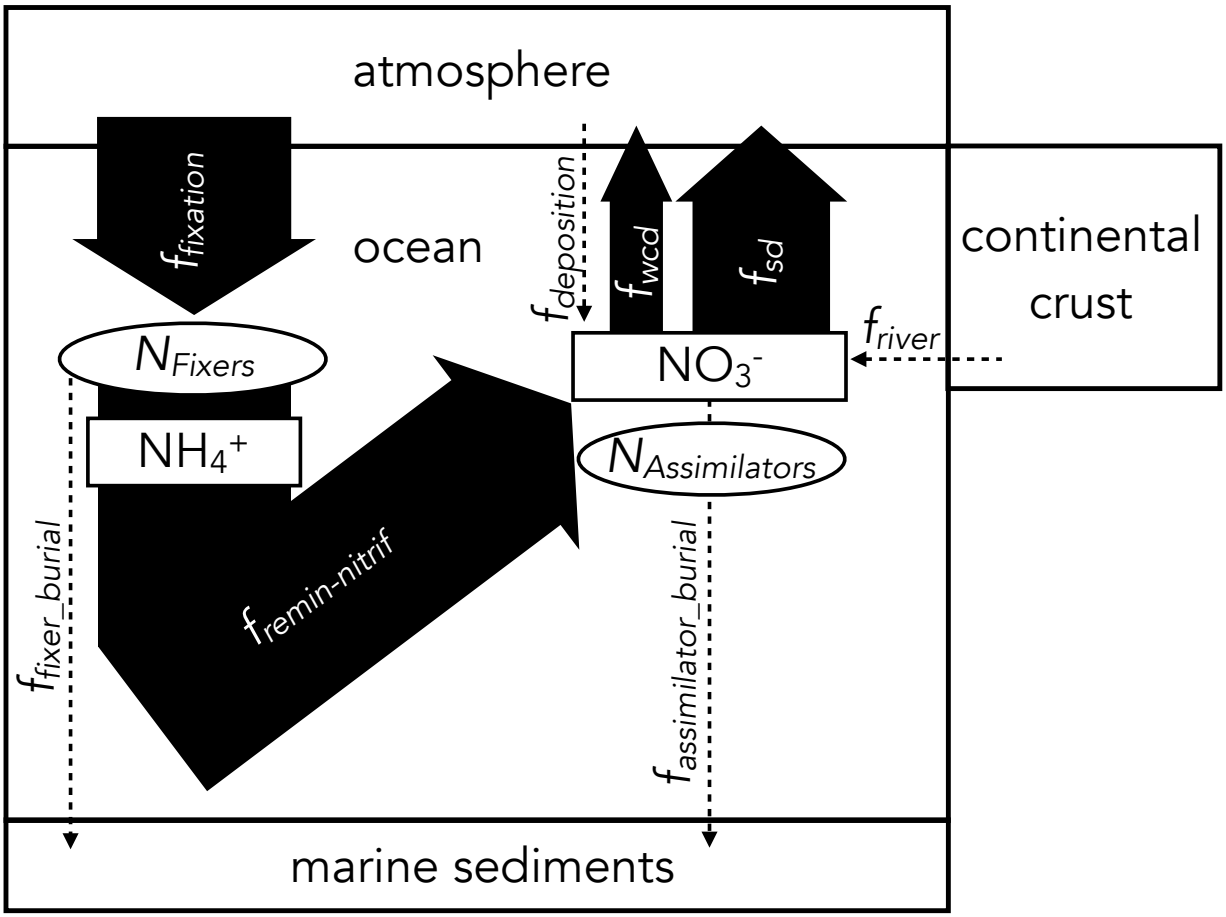

Figure 1. Box model schematic of Earth's surface nitrogen cycle. Nitrogen fixation ($f_{fixation}$) is the dominant input to the ocean system, with water column (f_{wcd}) and sediment (f_{sd}) denitrification constituting the major output fluxes. The dominant input (>99%) of nitrate is nitrification ($f_{remin\text{-}nitrif}$), with atmospheric deposition ($f_{deposition}$) and riverine (f_{river}) inputs comprising only minor contributions (<1%). Modern flux constants were used to calibrate the model, and then the balance of f_{wcd}, f_{sd}, and f_{burial} (including burial of both fixers and assimilators) was adjusted to simulate changes in ocean redox chemistry. Since remineralization of organic matter produces a small or negligible N isotope fractionation, ammonium burial with clay minerals is not treated separately in the model. A detailed description of model architecture can be found in the Supplementary Materials.

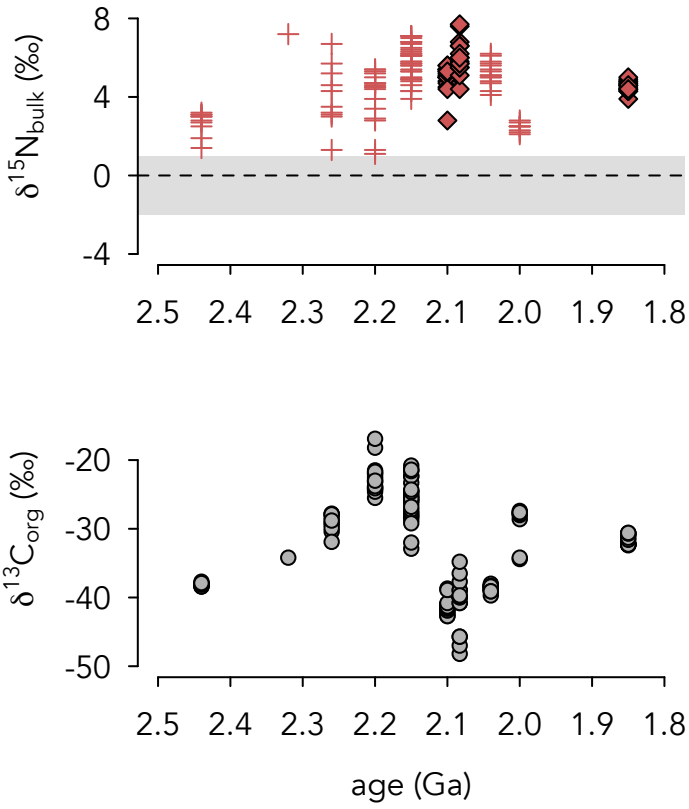

738

739 **Figure 2. $\delta^{15}N_{bulk}$ (top) and $\delta^{13}C_{org}$ (bottom) values of samples analyzed in this study.** Crosses denote nitrogen
740 isotope data from units that experienced lower greenschist facies metamorphism, diamonds denote data from units
741 that remained below greenschist facies. All nitrogen isotope data are enriched above the range of values expected
742 for nitrogen-fixation dominated systems (-2‰ to +1‰; grey shaded region). Most units contain carbon isotope ratios
743 that are depleted below the normal range for marine phytoplankton (-26‰ ± 7‰; Schidlowski, 2001), perhaps
744 reflecting heterotrophic degradation of sedimentary organic matter in anoxic seawater and sediments.

745
746

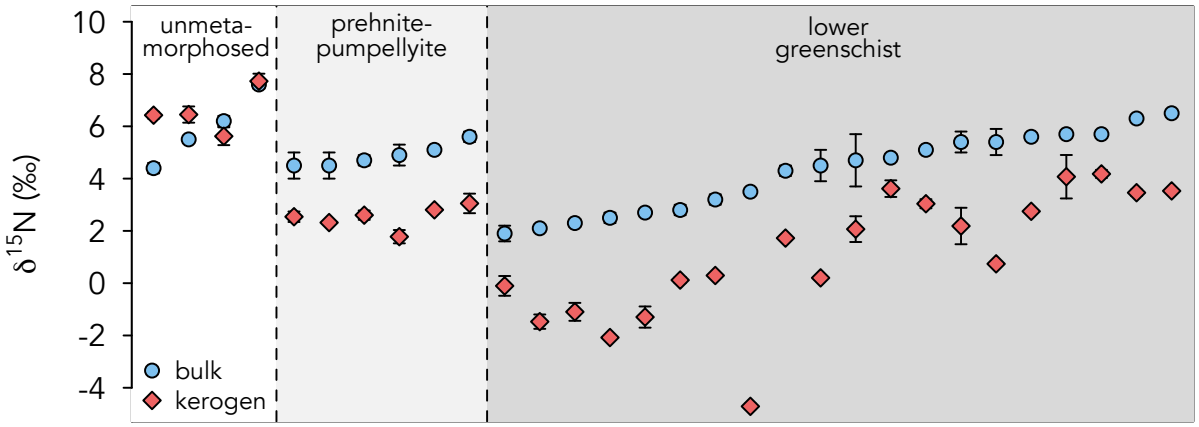

747
748 **Figure 3. Comparison of $\delta^{15}N_{bulk}$ and $\delta^{15}N_{ker}$ values for individual samples (error bars = 1σ).** The $\delta^{15}N_{ker}$ values show
749 a trend of being consistently isotopically lighter than their corresponding $\delta^{15}N_{bulk}$ values, which is consistent with a
750 previous study (Stüeken et al., 2017). Furthermore, the isotopic offset tends to be larger at higher metamorphic
751 grade, which corroborates the suggestion that isotopic re-equilibration occurs between nitrogen phases under
752 progressive metamorphism. The isotopic offsets observed in the samples are consistent with the metamorphic
753 grades that have been inferred from mineral assemblages.
754

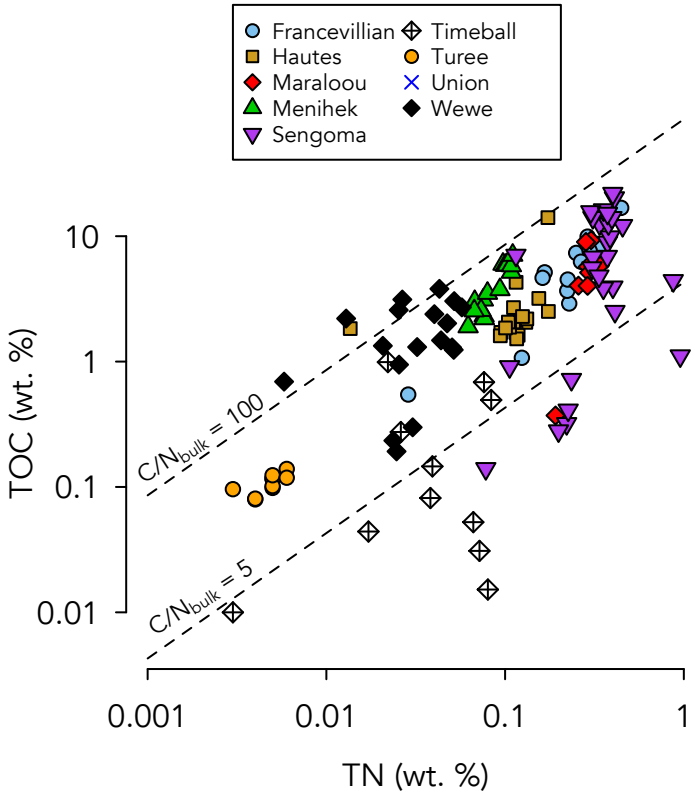

Figure 4. Total organic carbon versus total nitrogen values for all bulk-rock measurements in this study. Dotted lines show C/N ratios of 5 and 100, respectively. The average molar C/N ratio of planktonic biomass in the modern ocean is ~7 (Redfield, 1934). Water-column and sedimentary diagenesis can increase sedimentary C/N ratios, giving a spread in values similar to what is observed in most units in this study. Causes for low sedimentary C/N ratios are discussed in Section 5.1 of the main text.

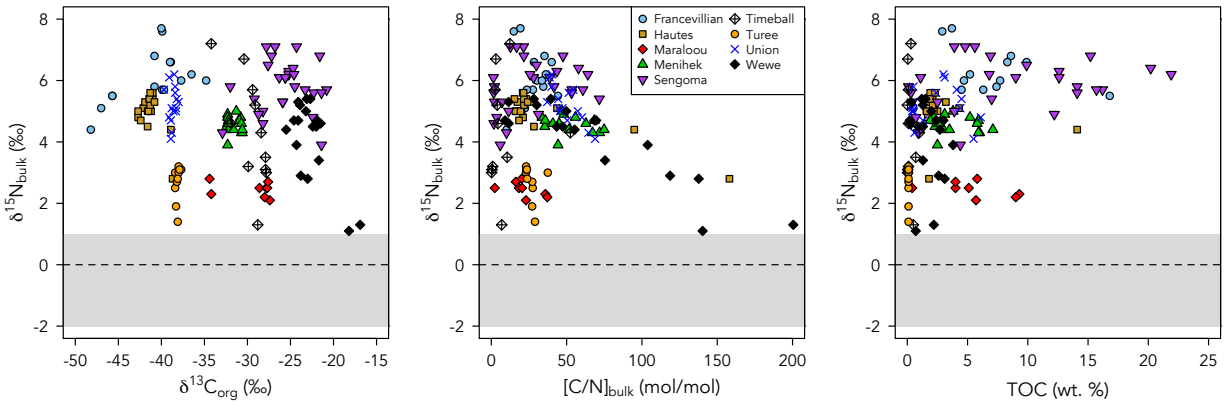

763

764 **Figure 5. Cross-plot assessment of the preservation of primary nitrogen isotope ratios.** Grey shaded region denotes
765 $\delta^{15}N_{bulk}$ values associated with nitrogen fixation-dominated ecosystems. The lack of co-variation between $\delta^{15}N_{bulk}$
766 and $\delta^{13}C_{org}$, C/N, and TOC suggests that the $\delta^{15}N_{bulk}$ values were not strongly affected by diagenetic and metamorphic
767 overprinting. See discussion for further details and Figs. S1-S3 for plots of individual units.

768

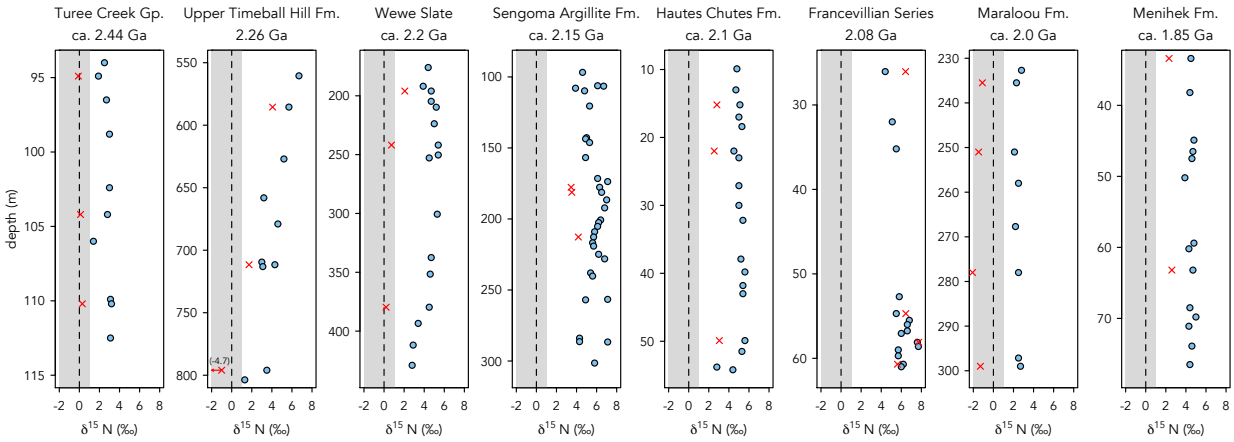

769

770 **Figure 6. Nitrogen isotope values plotted along stratigraphic profiles.** Circles show bulk-rock data, crosses denote
771 kerogen isolates. All studied units show $\delta^{15}N_{bulk}$ values that are consistently above the values expected for a fully
772 anaerobic, fixation-dominated ecosystem (grey shaded region). Outcrop samples from the Union Island Group are
773 not plotted as they were collected from multiple outcrops.

774

775

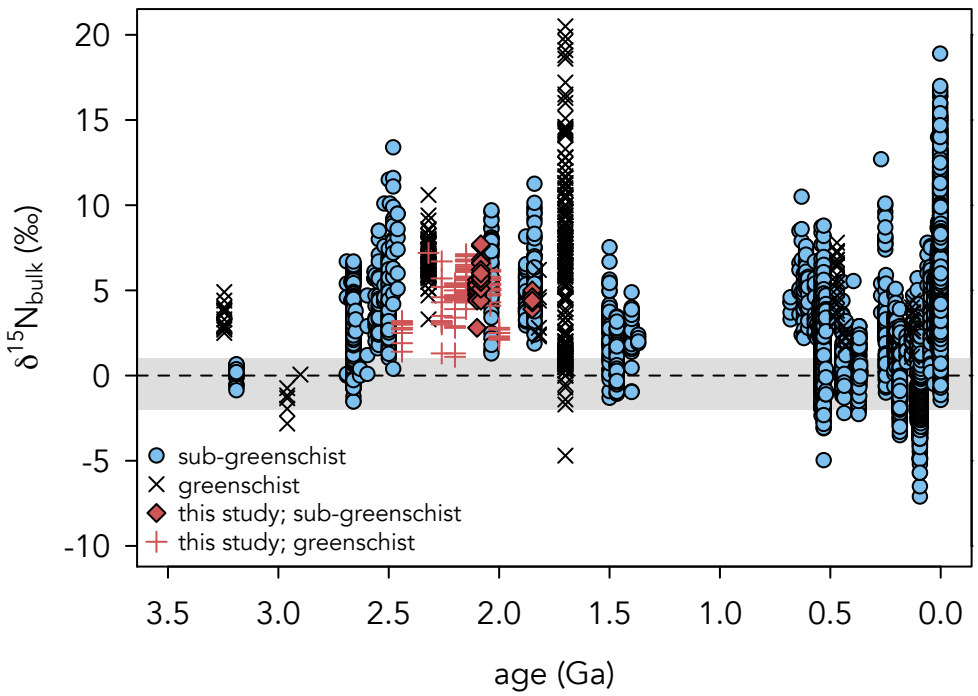

776

777 **Figure 7. Bulk-rock δ^{15}N values of marine sedimentary rocks through geologic time.** Consistently positive δ^{15}N
778 values in Paleoproterozoic shales imply that oxic conditions were prevalent in surface waters for hundreds of millions
779 of years after the onset of the Great Oxidation Event.

780

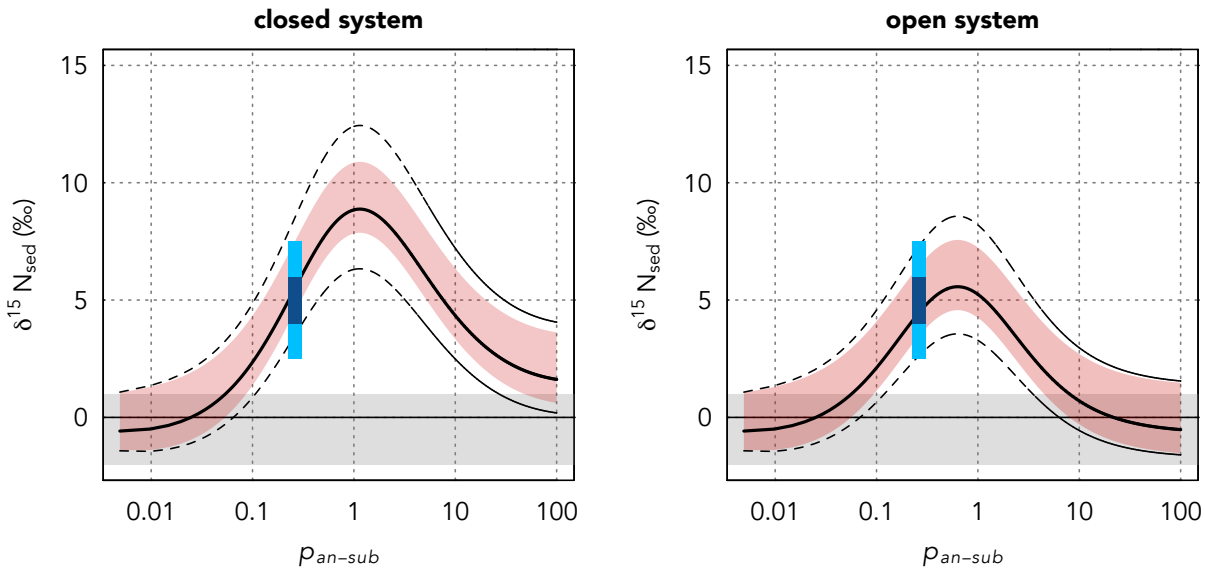

Figure 8. Modeled bulk-rock sedimentary $\delta^{15}N$ values under closed (left) and open (right) system dynamics, as a function of anoxia-to-suboxia extent ($p_{an\text{-}sub}$) in the upper ocean. Anoxia-to-suboxia is defined here as seawater with <4.5 µM of dissolved O_2 (see Supplementary Materials for discussion), where $p_{an\text{-}sub}$ = 100 corresponds to a globally anoxic ocean, and the modern ocean has a $p_{an\text{-}sub}$ value of 0.3. The mode in the $\delta^{15}N$ values of modern marine sediments is shown with a dark-blue bar (Tesdal et al., 2013); the lighter-blue bar corresponds to the 1σ range. Red-shaded region shows uncertainty interval derived from the range of isotopic fractionations associated with biological N_2-fixation. Black dashed lines show cumulative uncertainty interval including upper and lower limits on net isotopic effect of water column denitrification. Grey band denotes isotopic range of nitrogen fixation-dominated ecosystems.

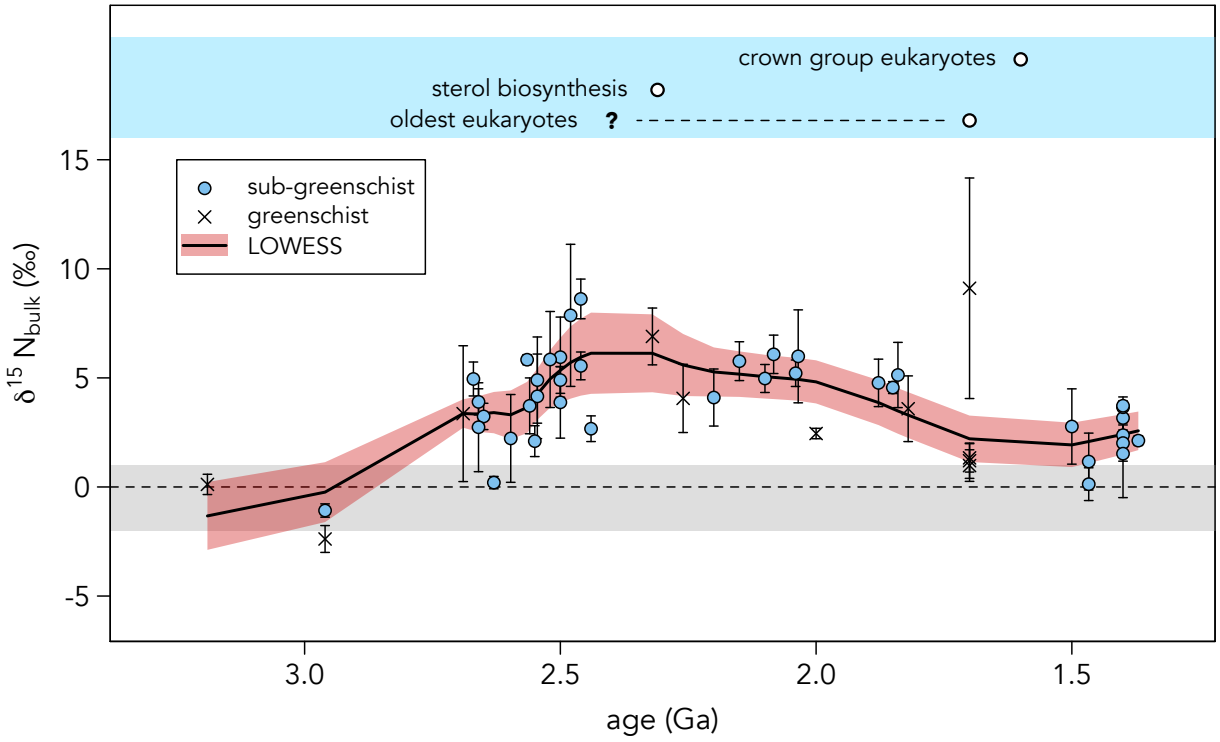

792

793 **Figure 9. Archean and Paleoproterozoic nitrogen isotope record and constraints on early eukaryotic evolution.**
794 Points are mean $\delta^{15}N$ values for individual formations with 1σ error bars. Black line is LOWESS curve, with 1σ
795 confidence interval shown in red shaded region. LOWESS calculations utilized a *d* value of 1 (local fits via linear
796 regression) and an *f* value of 0.3 in order to investigate long-term (~10^8 yr) trends. References for evolutionary events
797 are discussed in Section 5.4 of the text.

798